INFLUENCE OF SUPPORT PHASES ON THE NICKEL CATALYSED SELECTIVE HYDROGENATION OF CINNAMALDEHYDE

M. G. Prakash,[a,b] R. Mahalakshmy,[b] K. R. Krishnamurthy[a] and B. Viswanathan[a]*

Keywords: Cinnamaldehyde; hydrogenation; role of supports; polymorphs of titania; nickel at interface

Ni (15% w/w) supported on alumina, silica, and titania (P-25, anatase and rutile phases) have been investigated for the liquid phase hydrogenation of cinnamaldehyde. XRD, TPR and XPS data (binding energy shifts for Ni_{2p}) indicate metal-support interactions in all supported catalysts. Weaker binding of H_2 on Ni/TiO_2 (H_2-TPD) improves activity. Ni/TiO_2 phases display higher cinnamaldehyde conversion and selectivity to cinnamyl alcohol compared to the catalysts supported on alumina and silica. Amongst the three polymorphs of titania, the maximum activity, and selectivity displayed by Ni/ TiO_2-P-25, is attributed to the active Ni crystallites located at the interface between anatase and rutile phases in titania P-25 matrix (HRTEM). Though Ni crystallites on alumina and silica are relatively smaller (compared to those on the three TiO_2 phases) in size, their activity vis-à-vis for those supported on titania phases is less, implying that factors other than crystallite size influence the performance.

*Corresponding authors
Dr. B. Viswanathan
E-mail: bvnathan@iitm.ac.in
[a] National Centre for Catalysis Research (NCCR), Indian Institute of Technology, Madras, Chennai-600036, India.
[b] Department of Chemistry, Thiagarajar College, Madurai Kamaraj University, Madurai-625009, India.

INTRODUCTION

Selective hydrogenation of cinnamaldehyde (CAL) to cinnamyl alcohol (COL) and hydrocinnamaldehyde (HCAL) is a key step in the synthesis of fine chemicals for pharmaceutical and fragrance applications.[1] Formation of COL by a preferential hydrogenation of the C=O group is not favoured, because the hydrogenation of C=C double bond, leading to the formation of HCAL, is thermodynamically favoured by 35 kJ mol^{-1} and the kinetics of hydrogenation also favours this route.[2] Conventionally, hydrogenation of C=O bond in CAL is achieved by reduction with various hydride donors, such as $LiAlH_4$ and $NaBH_4$.[3-5] Development of non-noble metal catalysts with high activity and selectivity towards COL remains a challenge.[6,7] Supported noble metal (Pt, Pd, & Ir) catalysts have been studied extensively for this reaction. Selectivity towards COL is significantly influenced by several factors such as metal particle size,[8-11] nature of support,[12] promoters[13] and solvents.[14]

A number of supports like titania, zirconia, silica, and alumina have been explored for the selective hydrogenation of CAL. Reducible supports like TiO_2, Nb_2O_5 are known to promote SMSI effect, which helps in achieving higher selectivity to COL.[15-16] Graphene oxide supported Pt catalysts display high selectivity for COL (85.3%).[17] Graphene increases electron density around Pt, which does not favor adsorption of CAL via C=C bond and hence the improvement in COL selectivity. Xiaonian Li et al.[18] have reported COL selectivity of 83.8% on Au/TiO_2 and 55.6% on Ir/TiO_2. While Co supported on TiO_2 exhibits COL selectivity of 58.8%, the selectivity increases to 74-83 % when ZSM-5 is used as support.[19,20] Marchi et al.[21] have studied liquid phase hydrogenation of cinnamaldehyde over Cu/SiO_2, Cu-Al, Cu-Zn-Al, Cu-Ni-Zn-Al and Cu-Co-Zn-Al oxide catalysts and observed selectivity of 10-52.9% for COL.

TiO_2 supported catalysts significantly enhance the rate of C=O hydrogenation over Pt, Ni, Co metals, although the hydrogenation of C=C double bonds or aromatic rings have not been observed.[22-24] Reducibility of TiO_2 results in the formation of oxygen deficient TiO_{2-x} phase containing Ti^{3+} ions, which tend to polarize C=O, leading to higher selectivity towards COL.[25]

Phase composition and polymorph character of the supports, which define the location/environment of active phases/metals play crucial role in controlling activity and selectivity.[26] In order to investigate these specific aspects, a systematic study has been carried out on Ni-based catalysts supported on different supports like, alumina, silica, different polymorphs of titania, namely, anatase, rutile and mixed phase containing anatase & rutile (titania P-25) towards selective hydrogenation of CAL. To the best of our knowledge, there are no reports on the influence of such supports on Ni-based catalysts for hydrogenation of CAL.

EXPERIMENTAL

TiO_2-P-25 (Evonik), TiO_2 anatase (Hombikat), Pural (Sasol), SiO_2 (Evonik) were commercial samples and used as such. TiO_2-Rutile sample from Aldrich was used as such. $Ni(CH_3COO)_2.4H_2O$ (CDH), NaOH (SRL), D-glucose (Merck), methanol, liquor ammonia (Qualigens) and cinnamaldehyde (Aldrich) were used as such. Pural (pseudo-boehmite) was calcined at 450°C in air for 4 h to get gamma alumina support.

Preparation of supported nickel catalysts

All catalysts were prepared by chemical reduction of nickel acetate, using D-glucose as reducing as well as capping agent.[27] Nickel nanoparticles, stabilized in alkaline medium, were anchored onto different supports. Typically, 0.74 g of Nickel acetate and 40 ml of D-glucose solution (0.15 M) were mixed and stirred for 30 min at room temperature. 10 ml of liquor ammonia was added drop-wise to the mixture. Refluxing the mixture for 5 h at 80ºC turned its color to black indicating the reduction of Ni^{2+} ions to Ni. Then, 1 g of support (alumina/silica/TiO_2(P-25 type)/TiO_2-anatase/TiO_2-rutile) was added to the solution containing Ni nanoparticles and stirred for 2 h. The mixture was cooled to ambient temperature, centrifuged, washed with anhydrous ethanol and dried at 60 ºC for 24 h. All catalysts were pre-reduced in hydrogen gas flow at 300 °C for 2 h. All characterization and hydrogenation experiments were carried out with pre-reduced catalysts after appropriate pre-treatment procedures.

Characterization of catalysts

XRD measurements were carried out on a Rigaku Miniflex II powder X-ray diffractometer with a Ni-filtered CuKα radiation source (λ = 1.5406 Aº) operating at 30 kV and 15 mA. High angle (10 – 90°) diffraction patterns were obtained with a scanning rate of 3° min^{-1}. The crystallite size was calculated by X-ray line broadening method[28] using Debye-Scherrer equation (1).

$$d = K\frac{\lambda}{\beta\cos\theta} \qquad (1)$$

where

d is the crystallite size in *nm*,

K is the numerical (crystallite shape) constant (K = 0.89 in this case),

λ is the wavelength of radiation used (λ= 1.5405 Å),

β is full width at half maximum (FWHM) in radians

θ is the Bragg diffraction angle in degrees, at the peak maximum.

The surface morphology and composition of the support and deposited material were studied using a QUANTA 200-FEI instrument equipped with an METEK energy dispersive X-ray analysis (EDX) system. The sample in powdered form was spread on the carbon tape (adhesive tape, normally used in SEM measurements for conduction purpose) and mounted on the SEM sample holder and imaged.

Transmission electron micrographs were recorded on a Philips CM20 model (120 kV) and JEOL 3010 model (200KV). Few milligrams of the samples (1-2 mg) were dispersed in few mL (4-5 mL) of ethanol by ultrasonication for 30 minutes, and the sample was kept aside for 10 min. A drop of the top layer was placed on a carbon-coated copper grid and allowed to dry in air at room temperature. Image J software was used to calculate the crystallite sizes. Based on the mean crystallite size measured from TEM data, Ni metal dispersion (φ) was calculated using the formula (2)

$$\varphi = \frac{600M_{\mathrm{Ni}}}{\rho d_{\mathrm{nm}} a_{\mathrm{Ni}} N_{\mathrm{A}}} \qquad (2)$$

where

M is the molecular weight of metal in case,

a is the atomic surface area (3.8×10^{-20} m^2/atom for Ni),

ρ is the metal density (8.9 g/cm^3 of Ni),

N_a is Avogadro's number, and

d_{nm} is the average particle diameter estimated from TEM in nanometers.

TPR patterns for the catalysts were recorded in Micromeritics-Auto Chem II 2920 unit using argon (95 %) + hydrogen (5 %) mixture as the carrier gas. The hydrogen consumption was recorded with TCD cell. For TPR measurements, the catalysts (50 mg) were pretreated at 300 ºC in air (25 cm^3 min^{-1}) for 1 hour and then cooled to room temperature. Gas flow was changed to 5%H_2/Ar (25 cm^3 min^{-1}) at room temperature. After stabilization of the baseline, TPR was started from RT to 700 ºC @ 10 ºC min^{-1}.

Ni metal surface area measurements were performed by H_2 pulse chemisorption in the same unit. 50 mg of catalysts were pre-treated at 300 ºC in high purity Ar gas (25 cm^3 min^{-1}) for 1 h and then cooled to room temperature under Ar flow. The catalysts were reduced at 300 °C for 2 h under 10 % H_2/Ar flow, cooled down to RT under Ar. H_2 pulses were injected with Ar as a carrier gas until the eluted peak area of consecutive pulses was constant.

For H_2 TPD measurements, 50 mg of catalyst was reduced in hydrogen flow (25 cm^3 min^{-1}) at 300 °C for 4 h and cooled to ambient temperature. Ar flow (30 cm^3 min^{-1}) was then introduced, and the catalyst was purged for 30 min. After the stabilization of the baseline, TPD of H_2 was recorded up to 700 ^{0}C at a temperature ramp of 10 ^{0}C min^{-1}.

The metal content of the supported catalyst was estimated by ICP-OES (Perkin Elmer Optima Model 5300 DV) after calibration with a standard solution containing known metal content. The metal was extracted from the catalyst by boiling in aqua-regia.

Nitrogen adsorption-desorption isotherm measurements were carried out at 77 K using a Micrometrics ASAP 2020 surface area analyzer. Before adsorption, the samples were evacuated at 523 K for 12 h. The specific surface area of the samples was estimated using the Brunauer-Emmett-Teller (BET) method, and the pore size was calculated by Barrett-Joyner-Halenda (BJH) method. The pore volume was determined from the amount of nitrogen adsorbed at P/P_0= 0.95

The X-ray photoelectron spectroscopic studies were carried out using Omicron Nanotechnology instrument with MgK_α radiation. The base pressure of the analysis chamber during the scan was $2\cdot10^{-10}$ millibar. The pass energies for individual scan and survey are 20 and 100 eV, respectively. The spectra were recorded with the step width of 0.05 eV.

Performance evaluation of catalysts

Hydrogenation reactions were performed in liquid phase, in a 100 ml Parr reactor (Model-4848). The autoclave was charged with 150 mg of pre-reduced catalyst, 1.2 g of cinnamaldehyde and 16 ml of methanol. After purging first with nitrogen (three times) and then with hydrogen (three times) the autoclave was pressurized with hydrogen to the desired value of 20 kg/cm^2. The reactions were carried out for different catalysts at 120°C, for 1 h, with stirring rate of 600 rpm. No increase in conversion was observed at stirring rates higher than 600 rpm indicating that at this rate mass transfer limitations could be ruled out. The reaction products were separated by filtration and analyzed on Perkin Elmer Clarus-500 GC with ZB-1 capillary column and FID.

The experimental/process conditions mentioned above have been arrived at after carrying out a set of experiments aimed at optimization of reaction conditions. All the experiments for optimization were carried out with 15 % w/w Ni/TiO_2-P-25 catalyst.

RESULTS AND DISCUSSION

Ni contents in the final catalysts were checked by ICP-OES analysis and found to be 14.5-15.2 % w/w as per expectations.

X-ray diffraction

XRD patterns for nickel catalysts on three titania phases (Hombikat, Rutile, and P-25) in reduced form are shown in Fig. 1. Strong diffraction peaks at 2θ values 25.3º, 37º, 37.8º, 38.6º, 48.2º (anatase) and 27.5º, 36.2º, 39.4º, 41.3º, 44.1º (rutile) ascribed to the support TiO_2 and Ni crystallites with fcc structure at 2θ values 44.7º, 51.8º and 76.3º are observed. While the d-lines for P-25 & rutile phases are sharp, due to crystalline character, the d-lines for Hombikat are somewhat diffused and broad, indicating amorphous nature.

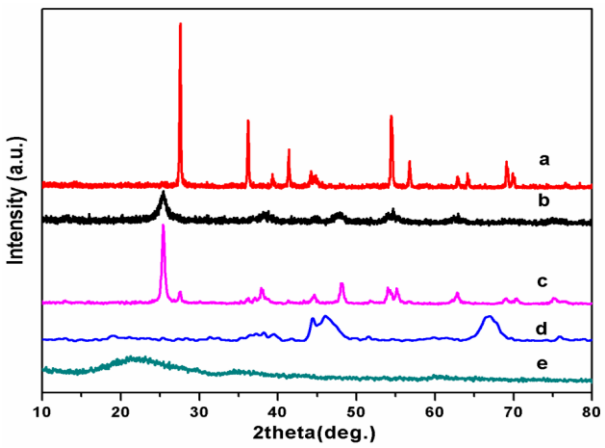

Figure 1. XRD Patterns for a) Ni/ TiO_2 Rutile b) Ni/ TiO_2 Hombikat c) Ni/ TiO_2 P-25 d) Ni/Al_2O_3 e) Ni/SiO_2.

Nickel was predominantly dispersed as Ni^0 on all the three supports. On the other hand, the XRD pattern for Ni/SiO_2 catalyst displays broad silica peak around 2θ = 23° indicating the amorphous character of silica. No d-lines due to Ni^0 could be observed, suggesting, that the nickel was finely dispersed on the surface of the silica support. XRD pattern of Ni/Al_2O_3 catalyst shows that the main diffraction peaks due to Al_2O_3 are shifted to lower angles, possibly due to the formation of $NiAl_2O_4$ with spinel structure.[29] It is clear that nickel particles are highly dispersed on the supports.

Temperature programmed reduction (TPR)

Both Ni/TiO_2 (rutile), and Ni/TiO_2 (P-25) catalysts (curves a and c in Fig. 2) exhibited similar reduction patterns, with a major reduction peak at 343°C, along with a shoulder at 225 °C. While the shoulder at lower temperature indicates the presence of small amount of free NiO, the peak at 343 °C corresponds to the reduction of dispersed NiO. Ni/TiO_2 (Hombikat, curve b) shows only one reduction maximum at 340 °C, due to dispersed NiO, followed by a negative peak, possibly due to the desorption of split over hydrogen from the support.

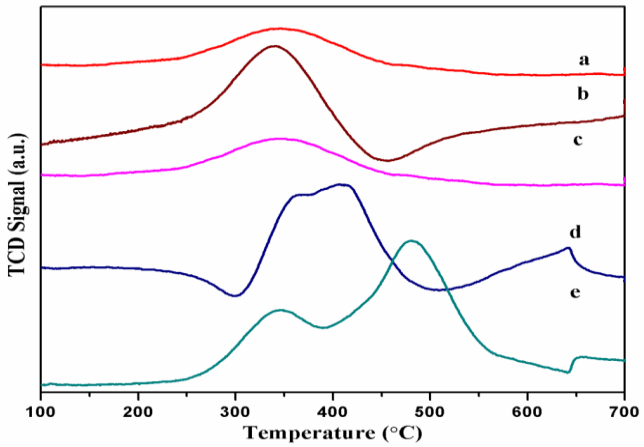

Figure 2. TPR profiles for a) Ni/Rutile b) Ni/Hombikat c) Ni/P-25 d) Ni/Al_2O_3 e) Ni/SiO_2.

High surface area and the presence of surface hydroxyl groups in Hombikat may have been responsible for the spill over. For Ni/Al_2O_3 catalysts (curve d), three reduction maxima are observed. The first peak at 362 °C is assigned to dispersed nickel oxide with weak interaction with support. The second peak around at 411 °C can be assigned to the typical reduction peak of Ni^{2+} that has interacted with the support alumina, possibly forming aluminate. The third peak around at 641 °C can be attributed to the reduction of nickel aluminate species. In the case of Ni/SiO_2 (curve e), besides a low temperature reduction peak at 343 °C which is attributed to the reduction of dispersed and weakly bound NiO particles, two more reduction peaks at higher temperatures at 482 and 655 °C are observed, which could be ascribed to the reduction of strongly bound Ni^{2+} in contact with the oxide support and possible nickel silicate like phase.[30] To summarize, TPR studies clearly show that the nature of the supports governs the reduction pattern and metal-support interactions in the case of nickel supported on different carriers.

Temperature programmed desorption of H_2 (H_2TPD)

In order to study the nature of adsorbed hydrogen, on Ni H_2-TPD studies were carried out. Fig. 3 shows the H_2-TPD patterns for the Ni catalysts on different carriers.

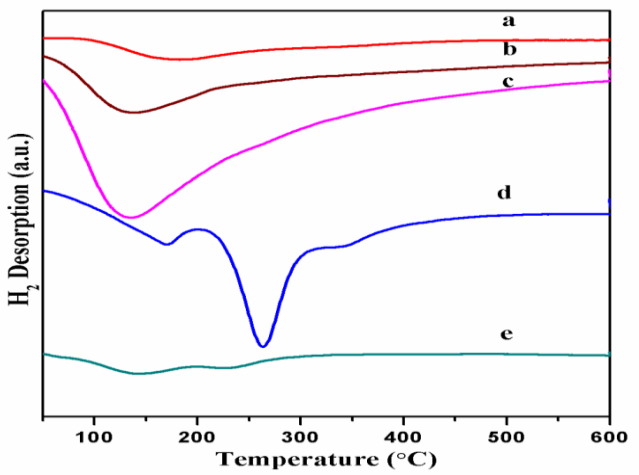

Figure 3. H_2-TPDprofiles for- a) Ni/Rutile b) Ni/Hombikat c) Ni/P-25 d) Ni/Al_2O_3 e) Ni/SiO_2

For all catalysts, a low-temperature desorption peak appears at 110- 160°C in the TPD profiles, which is usually attributed to the H_2 adsorbed on the Ni metal. Low-temperature desorption peak areas decrease in the following order: Ni/P25 > Ni/Hombikat > Ni/Rutile >Ni/SiO_2 > Ni/Al_2O_3 indicating that titania supported catalysts contain a larger fraction of reactive hydrogen. It is suggested that on Ni/TiO_2 (Hombikat, Rutile, and P25), bonding of hydrogen on Ni is weak and hence in the reactive state.[31] Low-intensity high temperatures desorption peaks around 210-270°C, possibly due to strongly chemisorbed hydrogen or the spillover of hydrogen atoms from metal to the support are also observed on Ni/SiO_2 and Ni/Al_2O_3 catalysts.[32] Additionally, Ni/Al_2O_3 displays one high temperature weak and broad desorption peak at 345°C. These higher temperature desorption peaks may be ascribed to the split over of hydrogen atoms from the Ni metal to the support, which recombine and desorb. The observed variations in H_2-TPD and TPR profiles indicate that the activation and spillover of hydrogen on the Ni catalyst surface are strongly affected by the properties of supports.

Scanning electron microscopy (SEM)

The morphology of reduced nickel catalysts on different supports was studied by SEM technique (Fig.4). Spherical shaped nano size nickel particles are observed for titania (Hombikat, P25, and Rutile) supported catalysts. In the case of Al_2O_3 and SiO_2 supported catalysts, no specific morphology is seen, but the certain degree of agglomeration of nano-sized particles is observed.

Transmission electron microscopy (TEM)

Representative TEM images of Ni/TiO_2 (Hombikat, Rutile, and P-25), Ni/Al_2O_3 and Ni/SiO_2 catalysts are shown in Fig.5. Ni/ TiO_2 P-25 catalyst shows a narrow particle size distribution, within a range of 7-10 nm. In the case of Ni/Hombikat and Ni/Rutile catalysts, particles with sizes ranging from 11-12 nm are observed. Smaller Ni crystallites, 7-9 nm, are observed in alumina and silica supported catalysts. Crystallite size of all catalysts are in the order: Ni/SiO_2 < Ni/Al_2O_3, < Ni/Hombikat < Ni/Rutile < Ni P-25, in agreement with the crystallite size values calculated by Scherrer formula based on the X-ray line broadening analysis. Ni metal dispersion and crystallite size values obtained by hydrogen chemisorption data are listed Table.1.

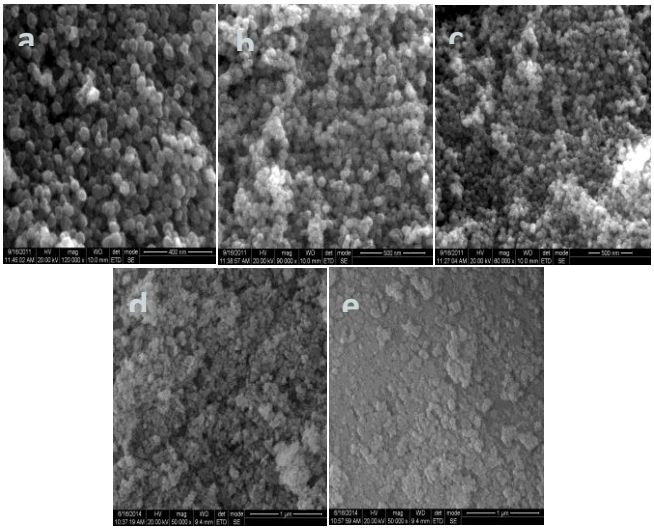

Figure 4. SEM images for a) Ni/Rutile b) Ni/Hombikat c) Ni/P-25 d) Ni/Al_2O_3 e) Ni/SiO_2

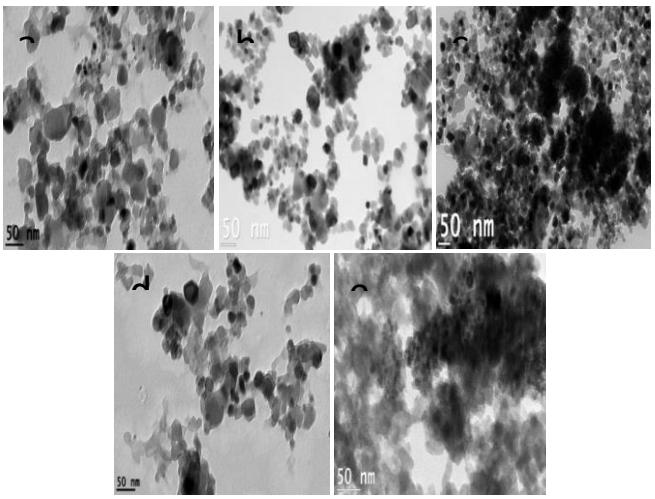

Figure 5. TEM images for a) Ni/Rutile b) Ni/Hombikat c) Ni/P-25 d) Ni/Al_2O_3 e) Ni/SiO_2

HRTEM image for Ni/TiO_2-P-25 is presented in Fig.6 wherein the prominent lattice fringes corresponding to (101) plane of anatase (0.35nm), (110) plane of rutile (0.32nm) phases in TiO_2-P-25 are observed along with those for (111) plane for fcc Ni crystallite (0.20nm). The micrograph clearly shows the presence of Ni crystallites in the interface between anatase and rutile phases of titania.

Table 1. Textural properties of nickel based catalysts

Catalyst	S_{BET}, $m^2 g^{-1}$	Pore volume, cm^3 g	Pore size, nm	Ni dispersion, %[a]	Ni crystallite size, nm		
					XRD	H_2	TEM
Ni/P25	50	0.20	16.1	9.5	10	10	9.8
Ni/Hombikat	311	0.33	5.0	8.9	8.8	12	11.7
Ni/Rutile	9.2	0.05	22.0	8.7	9.1	13	12.2
Ni/SiO_2	73	0.93	7.4	13.8	6.8	7.3	7.7
Ni/Al_2O_3	60	0.61	9.0	10.7	8.5	9.1	8.9

[a]-from H_2 chemisorption, XRD-XLBA, TEM

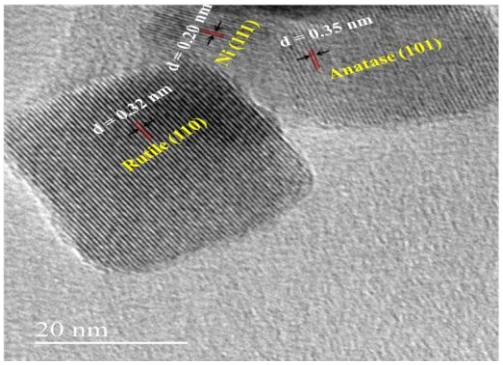

Figure 6. Lattice fringe image for anatase, rutile and Ni crystallites in Ni/TiO_2 P-25 catalyst

X-ray photoelectron spectroscopy (XPS)

On Ni catalysts supported on titania (P-25, Hombikat and Rutile) binding energy values for Ni $2p_{3/2}$ peaks were observed at 852.6 eV and 853.5 eV, which could be attributed to Ni^0 (metallic state) and residual Ni^{2+}species respectively[33] (Fig.7). In the case of Ni/SiO_2 $Ni2p_{3/2}$ peak for metallic Ni appears at 852.8 eV, with a slight shift with respect to the BE of metallic Ni. This may be due to the covalent interactions between Ni and Si catalysts.[34] The shift in the binding energy of Ni $2p_{3/2}$ peak observed for Ni/Al_2O_3 is consistent with the reported Ni $2p_{3/2}$ binding energy shift for $NiAl_2O_4$[35], which is in agreement with the XRD data.

N_2-Physisorption and H_2 pulse chemisorption

Textural properties, nickel dispersion and Ni particle size of supported Ni catalysts are listed in Table.1. The addition of 15 wt.% Ni metal to the corresponding support causes a slight change in the BET surface area, pore volume and average pore size. According to the H_2 pulse chemisorption results, the Ni/TiO_2 (Hombikat, Rutile and P25) catalysts have lower nickel dispersion than Ni/Al_2O_3 and Ni/SiO_2 catalysts.[36] TEM results on the catalysts corroborate this aspect.

Selective hydrogenation of cinnamaldehyde

The results on the selective hydrogenation of cinnamaldehyde (CAL) on Ni catalysts with different supports are given in Table 2. Ni/TiO_2 P25) displayed the highest CAL conversion (91%) with a maximum selectivity of 61% to COL. Hombikat and rutile titania supported Ni catalysts showed the moderate conversion of 57 % and 51 %, respectively but the selectivity towards COL was nearly half of the value (30.3 % and 24.4% respectively) displayed by the P-25 supported catalyst. Ni/SiO_2 and Ni/Al_2O_3 catalysts show still lower CAL conversion and COL selectivity. It is clear that the nature of the support and its morphology/polymorph character influences the activity and selectivity.

Table 2. Conversion and selectivity data for hydrogenation of cinnamaldehyde at 120 °C

Catalyst	CAL conv., %	Selectivity, %			
		HCAL	COL	HCOL	Others
Ni/P25	91	31	61	6.9	1.1
Ni/Hombikat	57	66	30.3	1.2	2.5
Ni/Rutile	51	72	24.4	1.0	2.6
Ni/SiO_2	38	79	18	0.8	2.2
Ni/Al_2O_3	18	78.8	17.2	0.6	3.4

Catalyst wt. -150 mg; COL-1.2 g, methanol-16 mL, pressure – 20 kg cm^{-2}, Reaction time – 1 h.

Among the three different types of supports, titania, alumina and silica, all the three titania supports display higher activity and selectivity vis-à-vis the other two types of supports. Reducibility of TiO_2 results in the formation of oxygen deficient TiO_{2-x} phase containing Ti^{3+} ions, which tend to decorate Ni crystallites and polarize C=O, leading to higher activity and selectivity towards COL. Small amounts of unreduced NiO present in the catalyst acts as Lewis acid sites, which also activates the C=O.[15] Superior performance of Co/TiO_2 compared to Co supported on alumina and silica supports[25] lends credence to this phenomenon. Though Ni crystallite size of alumina and silica are small, activity for CAL conversion and selectivity for COL are lower, compared to those on titania supports, implying that the crystallite size alone is not the key factor in determining the performance. Besides, some part Ni, present as nickel aluminate/silicate in alumina/silica supports, may not be available for the reaction.

Amongst the three polymorphs of titania, maximum activity and selectivity displayed by Ni-P-25 (Table 2) could be attributed to the active Ni crystallites located at the interface between anatase and rutile phases in titania P-25 matrix, as revealed by the HRTEM studies (Fig.6). The superior performance of active metals, located preferentially at the interface between two polymorphs in a support matrix, has been reported earlier.

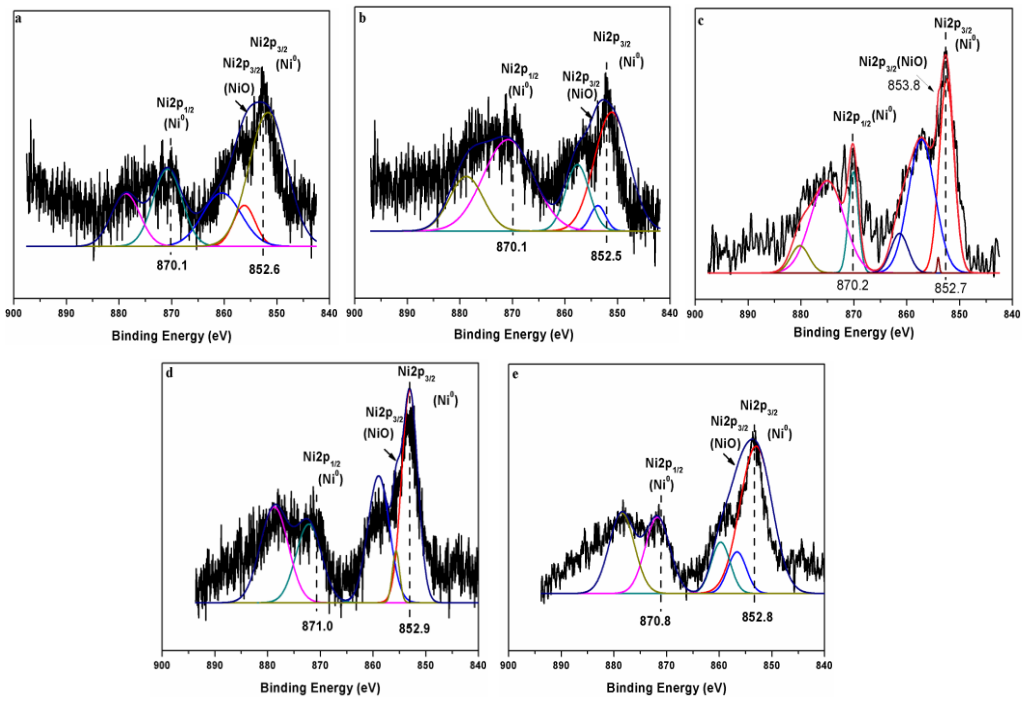

Figure 7. XPS spectrum for- a) Ni/Rutile b) Ni/Hombikat c) Ni/P-25 d) Ni/Al_2O_3 e) Ni/SiO_2.

Bin Wang et.al[37] have observed that Cu crystallites located at the interface between anatase and rutile phases in TiO_2 P-25 display high activity and selectivity for the hydrogenation of dimethyl oxalate to ethylene glycol. Wang et al. also observed that on pure anatase and rutile phases, in the absence of interfaces, Cu underwent agglomeration. Thus the presence of interfaces in P-25 helps in the activation as well as the dispersion of Cu. High activity of Au crystallites preferentially located at the interfaces in TiO_2 P-25 has been observed for the production of H_2 from ethanol-water mixtures.[38] Corresponding anatase, and rutile titania supported Au nanocrystals displayed lower activity. Synergistic electron transfer between the two polymorphs of titania and Au nanocrystals is proposed to be the reason for the high activity. Tsukomoto et al.[39] have reported that Au nanoparticles of size < 5 nm, located preferentially at the anatase –rutile interface in P-25, are highly active for the photocatalytic oxidation of alcohol. It is proposed that the catalyst architecture consisting of anatase-Au-rutile function as a joint active site, facilitating smooth electron transfer from Au to titania. In the present case, such preferential location of Ni nanoparticles in the interfaces (between anatase and rutile) within titania P-25 phase (Fig.6) could be responsible for the higher CAL conversion, and selectivity for COL observed with Ni/TiO_2P-25.

Conclusions

Nickel catalysts supported on alumina, silica and three different phases of titania (anatase, rutile & P-25) display distinct physicochemical characteristics that profoundly influence their activity and selectivity for hydrogenation of cinnamaldehyde. XRD and TPR data reveal that metal-support interactions are prominent in all supported catalysts. Morphology of titania supports influences the reduction behavior of the respective NiO phases. XPS studies indicate the presence of small amounts of unreduced NiO in all the five catalysts. Shifts in the XPS binding energy for Ni2p lines are indicative of metal-support interactions. H_2 TPD studies show that the bonding of hydrogen on titania supported catalysts is weaker and hence more reactive than that on alumina and silica supported catalysts. Nickel crystallite sizes measured by TEM and H_2 chemisorption studies fall in the narrow range of 7-12 nm. Catalysts supported on titania display higher CAL conversion and selectivity to COL in comparison with those supported on alumina and silica. Reducibility of TiO_2 leads to the formation of oxygen deficient TiO_{2-x} phase containing Ti^{3+} ions, which tend to decorate Ni crystallites and polarize C=O, leading to higher activity and selectivity towards COL. Small amounts of unreduced NiO acts as Lewis acid sites, which also activate the C=O. Amongst the three polymorphs of titania, maximum activity and selectivity displayed by Ni-P-25 titania could be attributed to the active Ni crystallites located at the interface between anatase and rutile phases in titania P-25 matrix.

Acknowledgements

The authors would like to express their gratefulness to the Dept. of Science & Technology, Govt. of India for establishing research facilities at NCCR. MGP is thankful to CSIR for the award of SRF scholarship. Authors acknowledge the supply of Hombikat TiO_2 (Anatase) by M/s Sachtleben Chemie, Germany and M/s.Evonik Industries, Germany for TiO_2-P-25

References

[1]Gallezot, P., Richard, D., *Catal. Rev. Sci. Eng*., **1998**, *40*, 81. http://dx.doi.org/10.1080/01614949808007106

[2] Mohr, C., Hofmeister, H., Radnik, J., Claus, P., *J. Am. Chem. Soc*., **2003**, *125*, 1905. http://dx.doi.org/10.1021/ja027321q CC

[3] Daimon, A., Kamitanaka, T., Kishida, N., Matsuda, T., Harada, T., *J. Supercritical Fluids*, **2006**, *37*, 215. http://doi.org/10.1016/j.supflu.2005.09.001

[4]Kluson, P., Cerveny, L., *Appl. Catal. A Gen*.,**1995**, 128, 13. https://doi.org/10.1016/0926-860X (95)00046-1

[5]Ponec, V., *Appl. Catal. A Gen*., **1997**, *149*, 27. https://doi.org/10.1016/S0926-860X (96)00250-5

[6]Singh, U. K, Vannice, M. A., *Appl. Catal. A Gen*., **2001**, *213*, 1. http://doi.org/10.1016/S0926-860X (00)00885-1

[7]Cerveny, L., Ruzicka, V., *Catal. Rev. Sci. Eng*., **1982**, *24*, 503. http://dx.doi.org/10.1080/03602458208079662

[8]Milone, C., Crisafaulli, R., Ingoglia, S. L., Galvagno, S., *Catal. Today*, **2007**, *122*, 341. http://doi.org/10.1016/j.cattod.2007.01.011

[9]Kartusch, C., Van Bokhoven, J. A., *Gold Bull*., **2009**, *42*, 343. http://dx.doi.org /10.1007/BF03214957

[10]Merlo, A. B., Machado, B. F., Vetere, V., Faria, J. L., Casella, M. L., *Appl. Catal. A. Gen*., **2010**, *383*, 43. http://doi.org/10.1016/j.apcata.2010.05.020

[11]Plomp, A. J., Vuori, H. A., Krause, O. I., de Jong, K. P., Bitter, J. H., *Appl. Catal. A Gen*., **2008**, *351*, 9. http://doi.org/10.1016/j.apcata.2008.08.018

[12]Jurvilliers, X., Schneider, R., Fort, Y., Ghanbaja, J., *Appl. Org. Metal. Chem.* **2003**, *17*, 161. http://dx.doi.org /10.1002/aoc.398

[13]Mahata, N., Concalves, F., Fernando, M., Pereira, R., Figueiredo, J. L., *Appl. Catal. A Gen*., **2008**, *339*, 159. http://doi.org/10.1016/j.apcata.2008.01.023

[14]Zhang, L., Winterbottom, J. M., Boyes, A. P., Raymahasay, S., *J. Chem. Technol. Biotechnol.*, **1998**, *72*, 264. http://dx.doi.org /10.1002/(SICI)1097-4660

[15]Prakash, M. G., Mahalakshmy, R., Krishnamurthy, K. R., Viswanathan, B., *Catal. Sci. Technol*., **2015**, *5*, 3313. http://dx.doi.org //10.1039/C4CY01379D

[16]Reyes, P., Rojas, H., Pecchi, G., Fierro, J. L. G., *J. Mol. Catal. A. Chem.*, **2002**, *179*, 293. http://doi.org/10.1016/S1381-1169(01)00409-5

[17]Shi, J., Nie, R., Chen, P., Hou, Z., *Catal. Commun*., **2013**, *41*, 101. http://doi.org/10.1016/j.catcom.2013.07.012

[18]Zhao, J., Ni, J., Xu, J., Xu, X., Li, X., *Catal. Commun*., **2014**, *54*, 72. http://doi.org/10.1016/j.catcom.2014.05.012

[19]Wu, Z., Zhao, J., Zhang, M., Li, W., Tao, K., *Catal. Commun*., **2010**, *11*, 973. http://doi.org/10.1016/j.catcom.2010.04.018

[20]Zhang, B., Zhang, X. B., Xu, L. Y., Zhang, Y. J., Qin, Y .H., Liang, C. F., *React. Kinet. Mech. Cat*., **2013**, *110*, 207. http://dx.doi.org /10.1007/s11144-013-0589-7.

[21]Marchi, A. J., Gordo, D. A., Trasarti, A. F., Aspesteguia, C. R., *Appl. Catal. A. Gen*., **2003**, *249*, 53. http://doi.org/10.1016/S0926-860X (03)00199-6

[22]Englisch, M., Jentys, A., Lercher, J. A., *J. Catal.*, **1997**, *166*, 25. https://doi.org/10.1006/jcat.1997.1494

[23]Bhogeswararao, S., Kumar, V. P., Chary, K. V. R., Srinivas, D., *Catal. Lett*., **2013**, *143*, 1266. doi:10.1007/s10562-013-1064-9

[24]Rudolf, C., Dragoi, B., Ungureanu, A., Chirieac, A., Royer, Nastro, S. A., Dumitriu, E., *Catal. Sci. Technol*., **2014**, *4*, 179. http://dx.doi.org /10.1039/C3CY00611E

[25]Raj, K. J. A., Prakash, M. G., Elangovan, T., Viswanathan, B., *Catal. Lett*., **2012**, *142*, 87. doi:10.1007/s10562-011-0693-0

[26]Ruppert, A. M., Grams, J., Je˛drzejczyk, M., Matras-Michalska, J., Keller, N., Ostojska, K., Sautet, P., *ChemSusChem*., **2015**, *8*, 1538. http://dx 10.1002/cssc.201403332

[27]Vasseem, M., Tripathy, N,, Khang, G., Halm, Y., *RSC. Adv*., **2013**, *3*, 9698. http://dx.doi.org /10.1039/C3RA40462E.

[28]Als-Nielsen, J., McMorrow, D., *Elements of Modern X-ray Physics*, John Wiley & Sons, Ltd., **2001**.

[29]Schefer, B., Heijeinga, J. J., Moulijn, J. A., *J. Phys. Chem*., **1987**, *91*, 4752., http://dx.doi.org /10.1021/j100302a023

[30]Liu, Y., Chen, J., Zhang, J., *Chin. J. Chem. Eng*., **2007**, *15*, 63. https://doi.org/10.1016/S1004-9541(07) 60034-2

[31]Amorima, C., Wang, X., Keane, M. A., *Chin. J. Catal*., **2011**, *32*, 746. http://dx.doi.org/10.1016/S1872-2067(10) 60228-8

[32]Braos-García, P., García-Sancho, C., Infantes-Molina, A., Rodríguez-Castellón, E., Jiménez-López, A., *Appl. Catal. A Gen.*, **2010**, *381*, 132. http://doi.org/10.1016/j.apcata.2010.03.061

[33]Grosvenor, A. P., Biesinger, M. C., Smart, R. St. C., McIntyre, N. S., *Surf. Sci*., **2006**, *600*, 1771. http://doi.org/10.1016/j.susc.2006.01.041

[34]Chen, X., Li, M., Xinkui, J., Williams, C. T., Liang, C., *Ind. Eng. Chem. Res*., **2012**, *51*, 3604. http://dx.doi.org /10.1021/ie202227j

[35]Heracleous, E., Lee, A. F., Wilson, K., Lemonidou, A. A., *J. Catal.*, **2005**, *231*, 159. http//doi.org/10.1016/j.jcat.2005.01.015

[36]Liu, N. Y., Feng, J. T., He, Y. F., Sun, J. H., Li, D. Q., *Catal. Sci. Technol*., **2015**, *5*, 1231. http://dx.doi.org /10.1039/C4CY01160K

[37]Wang, B., Wen, C., Cui, Y., Chen, X., Dong, Y., Dai, W. L, *RSC Adv.*, **2015**, *5*, 29040. http://dx.doi.org /10.1039/C5RA00053J

[38]Jovic, V., Chen, W. T., Sun-Waterhouse, D., Blackford, M. G., Idriss, H., Waterhouse, G. I. N., *J. Catal*., **2013**, *305*, 307. http://doi.org/10.1016/j.jcat.2013.05.031

[39]Tsukamoto, D., Shiraishi, Y. A., Sugano, S., Tanaka, S., Hirai, T., *J. Am. Chem. Soc*., **2012**, *134*, 6309. http://dx.doi.org/10.1021/ja2120647

Received: 19.03.2017.
Accepted: 30.04.2017.